Yan et al. Nanoscale Research Letters (2017) 12:363
DOI 10.1186/s11671-017-2131-8

Nanoscale Research Letters

NANO EXPRESS Open Access

Band Offset Measurements in Atomic-Layer-Deposited $Al_2O_3/Zn_{0.8}Al_{0.2}O$ Heterojunction Studied by X-ray Photoelectron Spectroscopy

Baojun Yan[1*], Shulin Liu[1], Yuekun Heng[1], Yuzhen Yang[1,2], Yang Yu[1,3] and Kaile Wen[1,4]

Abstract

Pure aluminum oxide (Al_2O_3) and zinc aluminum oxide ($Zn_xAl_{1-x}O$) thin films were deposited by atomic layer deposition (ALD). The microstructure and optical band gaps (E_g) of the $Zn_xAl_{1-x}O$ ($0.2 \le x \le 1$) films were studied by X-ray diffractometer and Tauc method. The band offsets and alignment of atomic-layer-deposited $Al_2O_3/Zn_{0.8}Al_{0.2}O$ heterojunction were investigated in detail using charge-corrected X-ray photoelectron spectroscopy. In this work, different methodologies were adopted to recover the actual position of the core levels in insulator materials which were easily affected by differential charging phenomena. Valence band offset (ΔE_V) and conduction band offset (ΔE_C) for the interface of the $Al_2O_3/Zn_{0.8}Al_{0.2}O$ heterojunction have been constructed. An accurate value of $\Delta E_V = 0.82 \pm 0.12$ eV was obtained from various combinations of core levels of heterojunction with varied Al_2O_3 thickness. Given the experimental E_g of 6.8 eV for Al_2O_3 and 5.29 eV for $Zn_{0.8}Al_{0.2}O$, a type-I heterojunction with a ΔE_C of 0.69 ± 0.12 eV was found. The precise determination of the band alignment of $Al_2O_3/Zn_{0.8}Al_{0.2}O$ heterojunction is of particular importance for gaining insight to the design of various electronic devices based on such heterointerface.

Keywords: Atomic layer deposition, X-ray photoelectron spectroscopy, Heterojunction, Microchannel plate

Background

Nano-thick oxide films with high resistance have attracted much attention as the most promising conductive layer for the applications of microchannel plate (MCP) as electron multiplier [1, 2], resistive memories [3], and electron-optical micro-electro mechanical systems (MEMS) [4]. A large research effort has been devoted to the novel idea of adjusting resistivity of such thin films due to the above-mentioned large potential applications in a special environment. MCP is a thin glass plate with thickness of about 500 μm consisting of several millions pores of a cylinder geometry with a 4–25-μm diameter and with a bias angle usually 5°–13° to the normal of the plate surface, and the high aspect ratio in each pore is about 20:1–100:1 [5, 6]. For recent MCP fabrication, two kinds of nano-thick layers are deposited on the MCP pore surfaces to conduct an electron multiplication function [1, 2]. The first layer is a conductive layer for supplying electrons, and the second layer is a secondary electron emission (SEE) layer for generating electrons. The three-dimensional surfaces and high aspect ratio of MCP should be firstly taken into consideration for depositing uniform thickness and composition of thin films. So far, the only effective approach growing high-quality thin films is the atomic layer deposition (ALD) technique based on sequential self-terminating gas-solid reactions [7].

ZnO is an n-type semiconductor with a direct bandgap of around 3.37 eV and a large exciton binding energy of 60 meV at room temperature [8, 9]. A lot of elements such as Mg [10, 11], Cd [12], Ga [13], W [14], and Mo [15] were used to doping in ZnO in order to tune its optical and electrical properties for special applications. In electron multiplier application, such as MCP, zinc aluminum oxide ($Zn_xAl_{1-x}O$) films have been investigated because of their thermal stability in a special

* Correspondence: yanbj@ihep.ac.cn
[1]State Key Laboratory of Particle Detection and Electronics, Institute of High Energy Physics of Chinese Academy of Sciences, Beijing 100049, People's Republic of China
Full list of author information is available at the end of the article

application environment and low cost of industrialization. The properties of $Zn_xAl_{1-x}O$ films can be controlled by changing the Al content, paving a way to design optoelectronic and photonic devices based on this material. Usually, high-resistivity $Zn_xAl_{1-x}O$ thin films as a conductive layer with x at the range of 0.7–0.85 have been applied in the field of electron multiplier [16]. For SEE layers, boron-doped diamond with hydrogen-terminated material has higher SEE coefficient than that of other traditional insulators. This provides a strong impetus for the development of electron multipliers. However, in the presence of degradation due to electron beam-induced contamination, these must be seriously regarded as preliminary [17]. From a practical point of view, two kinds of traditional insulators used as SEE layers in MCP are magnesium oxide (MgO) and Al_2O_3 thin films [18]. Although pure MgO has higher SEE coefficient than that of Al_2O_3, it is limited in the application on MCP because it is highly deliquescent and its surface is rather reactive with atmospheric moisture and carbon dioxide as demonstrated by our previous work [19], which probably results in degraded SEE performance. However, the physical and chemical properties of Al_2O_3 are very stable even after long-term exposure to the atmosphere. Therefore, Al_2O_3 is one of the most commonly used SEE materials in MCP application.

According to the structure of MCP, the Al_2O_3 and $Zn_xAl_{1-x}O$ thin films have different band gaps (E_g) resulting in band offsets in the heterointerface. Therefore, the determination of the band offsets at $Al_2O_3/Zn_xAl_{1-x}O$ interface is of importance because valence band offset (ΔE_V) and conduction band offset (ΔE_C) can deteriorate or promote SEE performance and also have a great influence on the performance of electron multiplier.

Generally, Kraut's method is widely used to calculate the valence band maximum (VBM) and the conduction band minimum (CBM) of semiconductor/semiconductor heterojunctions [20]. However, in the case of insulator/semiconductor or, in more serious cases, insulator/insulator heterojunctions, the positive charges generated during X-ray bombardment accumulate in the insulators and induce a strong modification of the kinetic energy of the emitted photoelectrons which is the so-called differential charging effect [21]. Although it is probably dealt with using a neutralizing electron gun [22], the use of C 1*s* peak recalibration [23], and zero charging method [24–26], a careful evaluation of the experimental result is necessary due to the differential charging effect during X-ray irradiation [19].

In this work, we will study the structure and optical E_g of $Zn_xAl_{1-x}O$ ($0.2 \le x \le 1$) thin films firstly, and then, we especially determine the ΔE_V and ΔE_C of the $Al_2O_3/Zn_{0.8}Al_{0.2}O$ heterojunction by using high-resolution X-ray photoelectron spectroscopy (XPS).

Methods

Sample Preparation

Several samples were used in this study: nine 80-nm-thick $Zn_xAl_{1-x}O$ samples ($0.2 \le x \le 1$) individually grown on n-Si (1 1 1) and quartz substrates, a 30-nm-thick Al_2O_3 grown on n-Si (1 1 1) substrate, and 3, 4, 5, 8 nm of Al_2O_3 on 80 nm of $Zn_{0.8}Al_{0.2}O$ grown on n-Si (1 1 1). The quartz substrates were ultrasonically cleaned in an ethanol/acetone solution and then rinsed in deionized water. The polished Si substrates were dipped in hydrofluoric acid for 30 s and then placed in an ALD chamber waiting for deposition. For $Zn_xAl_{1-x}O$ layer deposition, $ZnO:Al_2O_3$ ALD was carried out using diethylzinc (DEZ), trimethylaluminum (TMA), and deionized water as Zn, Al, and oxidant precursor, respectively. The Al_2O_3 ALD was performed using separate TMA and H_2O exposures with sequence $TMA/N_2/H_2O/N_2$ (150 ms/4 s/150 ms/4 s). The ZnO ALD was performed using separate DEZ and H_2O exposures following the sequence $DEZ/N_2/H_2O/N_2$ (150 ms/4 s/150 ms/4 s). The doping was carried out by substituting TMA exposure for DEZ. The Zn contents in the $Zn_xAl_{1-x}O$ layers were controlled by adjusting the ratio of the pulse cycles of DEZ and TMA, where the Zn content x was varied from 0.2 to 1 (pure ZnO) atom %. For $Zn_{0.8}Al_{0.2}O$ layer, the DEZ and H_2O pulses were alternated, and every fifth DEZ pulse was substituted with a TMA pulse. Ultrahigh purity nitrogen was used as a carrier and purge gas. The reaction temperatures were 200 °C. The detailed parameters are listed in Table 1.

Characterization

Optical transmittance spectra in a wavelength range from 185 to 700 nm were carried out by using a double-beam UV-Vis-IR spectrophotometer (Agilent Cary 5000) at room temperature in air. The crystal structure of the films were characterized by X-ray diffraction (XRD, Bruker D8) using Cu K_α radiation (40 kV, 40 mA, λ = 1.54056 Å). The film thickness was measured by Spectroscopic Ellipsometry (Sopra GES5E) where the incident angle was fixed at 75°, and the wavelength region from 230 to 900 nm was scanned with 5-nm steps. And the ellipsometric thicknesses of samples ALD03, ALD04, ALD05, and ALD06 were 3.01, 4.02, 5.01, and 8.01 nm, respectively. The XPS (PHI Quantera SXM) is used to analyze both the core levels (CLs) and valence band spectra of the samples. Charge neutralization was performed with an electron flood gun, and all XPS spectra were calibrated by the C 1*s* peak at 284.6 eV. In order to avoid differential charging effect, during the measurement, the spectra were taken after a few minutes of X-ray irradiation. All the samples are measured under the same conditions in order to acquire reliable data.

Table 1 Detailed parameters for $Zn_{0.8}Al_{0.2}O$ and Al_2O_3 layers

Sample no.	Substrate	Material	Thickness (nm)	Composition	Characterization
ALD01	n-Si (111), quartz	$Zn_{0.8}Al_{0.2}O$	80	Zn:Al = 4:1 (atomic ratio)	XPS, XRD and UV-Vis
ALD02	n-Si (111)	Al_2O_3	30	Pure	XPS
ALD03	n-Si/ALD01	Al_2O_3	3	Pure	XPS, SE
ALD04	n-Si/ALD01	Al_2O_3	4	Pure	XPS, SE
ALD05	n-Si/ALD01	Al_2O_3	5	Pure	XPS, SE
ALD06	n-Si/ALD01	Al_2O_3	8	Pure	XPS, SE

Calculations

The ΔE_V of the $Al_2O_3/Zn_{0.8}Al_{0.2}O$ heterojunction can be calculated from Kraut's formula

$$\Delta E_V = \left(E_{CL}^{Zn_{0.8}Al_{0.2}O}(y) - E_{VBM}^{Zn_{0.8}Al_{0.2}O}\right) - \left(E_{CL}^{Al_2O_3}(x) - E_{VBM}^{Al_2O_3}\right) - \Delta E_{CL} \quad (1)$$

where $\Delta E_{CL} = \left(E_{CL}^{Zn_{0.8}Al_{0.2}O}(y) - E_{CL}^{Al_2O_3}(x)\right)$ was the energy difference between feature y and feature x CLs, which were measured by XPS measurement in the heterojunction sample, and $\left(E_{CL}^{Al_2O_3}(x) - E_{VBM}^{Al_2O_3}\right)$ and $\left(E_{CL}^{Zn_{0.8}Al_{0.2}O}(y) - E_{VBM}^{Zn_{0.8}Al_{0.2}O}\right)$ were the Al_2O_3 and $Zn_{0.8}Al_{0.2}O$ bulk constants, which were obtained on the respective thick films. The VBM values were determined by linear extrapolation of the leading edge to the baseline of the valence band spectra. A root sum square relationship is used to combine the uncertainties in the different binding energies to determine the uncertainty of calculated results [26].

Results and Discussion

Structure and Band Gaps of $Zn_xAl_{1-x}O$ Samples

The XRD patterns of the as-deposited 80-nm-thick $Zn_xAl_{1-x}O$ ($x = 0.2, 0.6, 0.8, 0.9, 1$) thin films grown on quartz and Si substrates are shown in Fig. 1a, b, respectively. For the pure ZnO grown on quartz substrates in Fig. 1a, the strong peaks at 32.4° and 34.8° and the relatively weak peaks at 36.5° and 57.2° come from hexagonal ZnO phase, indicating the polycrystalline nature of the ZnO layer. And strong (0 0 2) peak shows the preferential orientation growth of ALD ZnO. However, the above characteristic peaks become weak for $Zn_{0.9}Al_{0.1}O$ sample and disappear for $Zn_xAl_{1-x}O$ ($x \le 0.8$) samples, which suggests that ZnO crystallization is suppressed with Al concentration increase. Besides, the broad peak ranging from 20° to 30° is the typical pattern of the quartz substrate. For Si substrate, the strong peaks around 28.4° and 58.9° are easily detected (data not shown). These peaks are corresponding to the diffractions originated from Si (1 1 1) and Si (2 2 2) crystal planes. In addition, the relatively weak peaks in Fig. 1b at $2\theta = 32.6°$, 33.2°, 35.4°, 35.9°, 38.8°, 39.2°, and 42.8° in the diffractograms that arise from the Si substrate itself are also observed. These unknown peaks may be related to the process conditions for producing crystalline silicon and are observed in previous work [27, 28]. Except for diffraction peaks from the Si substrate, no other diffraction peaks from the $Zn_xAl_{1-x}O$ ($x \le 0.9$) samples are detected. Only (0 0 2) and weak (1 1 0) peaks appear in the pure ZnO sample. From the above results, the crystal quality of the $Zn_xAl_{1-x}O$ film is a serious decline with the increasing concentration of Al content. It is well known that the particle size of Al ions is less than that of Zn ions. Zn is easily substituted by Al when doping concentration of Al increases. This results in weakened ZnO crystallinity, so the structure of $Zn_xAl_{1-x}O$

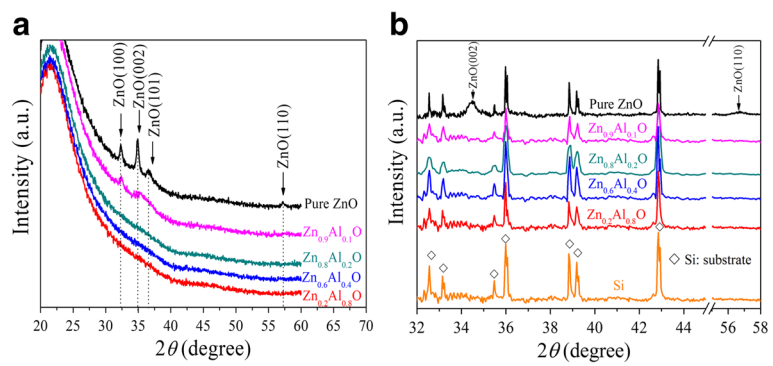

Fig. 1 XRD patterns of $Zn_xAl_{1-x}O$ samples deposited on **a** quartz substrate and **b** Si substrate

($x \leq 0.8$) samples is amorphous, in good agreement with previous results [29]. Taken into consideration, $Zn_xAl_{1-x}O$ layer growth appears to be substrate sensitive and Al doping concentration has an influence on the crystallization of the films.

Figure 2a shows transmission spectra of the $Zn_xAl_{1-x}O$ samples deposited on quartz substrate. The average transmittance is above 80% in the visible wavelength for all samples. It is found that ZnO film exhibits abrupt absorption edge which appears at ~390 nm corresponding to the fundamental E_g of ZnO. A blue shift of the absorption edge is apparently observed when Al concentration increases. The E_g of $Zn_xAl_{1-x}O$ thin films can be obtained by fitting the sharp absorption edges. The relationship between absorption coefficient (α) and E_g of direct band gap semiconductor is given by Tauc equation [30], $(\alpha h\nu)^2 = B(h\nu - E_g)$, where $h\nu$ is the photon energy and B is a constant. The dependence of $(\alpha h\nu)^2$ on photon energy is shown in Fig. 2b. The E_g is obtained by the extrapolations of the liner regions of the optical absorption edges. The E_g of pure ZnO thin film deposited by ALD is 3.26 eV, which is consistent with the previous reports [31, 32]. With the Zn concentration x decreases from 0.9 to 0.2, the E_g of $Zn_xAl_{1-x}O$ thin films increases from 4.11 to 6.51 eV. It is directly demonstrated that the E_g of $Zn_xAl_{1-x}O$ thin films can be adjusted in a large range by controlling the Al doping concentration, which makes it a suitable candidate for application in many scientific research fields [33, 34]. For the new type of MCP, the properties of $Zn_{0.8}Al_{0.2}O$ thin film are suitable for conductive layer proved by previous study [2]. Therefore, the E_g of atomic-layer-deposited $Zn_{0.8}Al_{0.2}O$ thin film is 5.29 eV, which is sufficient to make a band gap discontinuity in $Al_2O_3/Zn_{0.8}Al_{0.2}O$ heterojunction and is used for calculating the ΔE_C value later.

Valence and Conduction Band Offset Measurements of $Al_2O_3/Zn_{0.8}Al_{0.2}O$ Heterojunction

The XPS spectra of survey scan, CLs, and VBM region for $Zn_{0.8}Al_{0.2}O$ and Al_2O_3 samples are shown in Fig. 3. In this study, we find that the CLs positions of the $Zn_{0.8}Al_{0.2}O$ and Al_2O_3 thin films do not change as a function of X-ray irradiation time for 15 min (data not shown), because of operating a low energy electron flood gun. Figure 3a, e shows the whole scanning spectrum of the thick $Zn_{0.8}Al_{0.2}O$ and Al_2O_3 thin films, respectively. The C 1*s* peak at 284.6 eV appeared due to some surface contamination, and the Ar 2*p* peak at 242.1 eV appeared because of residual inert gas composition in the ultra-high vacuum chamber. The peaks in Fig. 3a located 660, 652, 582, 573, 559, 495, and 472 eV are Auger lines of Zn element. The stoichiometry of the thick films are checked by the ratio of the integrated area of Zn 2*p* peak to Al 2*p* peak for the $Zn_{0.8}Al_{0.2}O$ sample and Al 2*p* peak to O 1*s* peak for the Al_2O_3 sample. Both are corrected by corresponding atomic sensitivity factors *S* [35], taking into account their corresponding photoionization cross-sections of CLs calculated by Scofield [36], and the mean free path of the photoelectrons calculated by Tanuma et al [37]. Here, the *S* values are calculated to be 0.256, 2.768, and 0.733 for Al 2*p*, Zn $2p_{3/2}$, and O 1*s*. The atomic ratios Zn:Al = 3.97:1.01 for $Zn_{0.8}Al_{0.2}O$ and Al:O = 1.99:3.01 for Al_2O_3 compare well with that of designed ratio of atomic layer deposition, which indicate good stoichiometry of the $Zn_{0.8}Al_{0.2}O$ and Al_2O_3 layers. The high-resolution scans of Zn $2p_{3/2}$ and Zn $2p_{1/2}$ CLs of $Zn_{0.8}Al_{0.2}O$ are shown in Fig. 3b, c. The peaks fitted using Shirley backgrounds and Voigt (mixed Lorentzian-Gaussian) functions located 1021.41 and 1044.51 eV in Fig. 3b, c correspond to the electronic states of Zn $2p_{3/2}$ and Zn $2p_{1/2}$, respectively, and both are fitted by a single contribution, attributed to the bonding configuration Zn-O. The Al 2*p* peak of Al_2O_3 located 74.35 eV and O 1*s* peak located 531.1 eV are shown in Fig. 3f, g. The Al 2*p* spectrum as fitted by a single contribution, attributed to the bonding configuration Al-O. However, for the O 1*s* spectrum, an additional peak low-intensity higher binding energy component is also observed. This extra component is attributed to both O-Al and O-H bonds [38]. The VBM positions are determined by a linear extrapolation of the

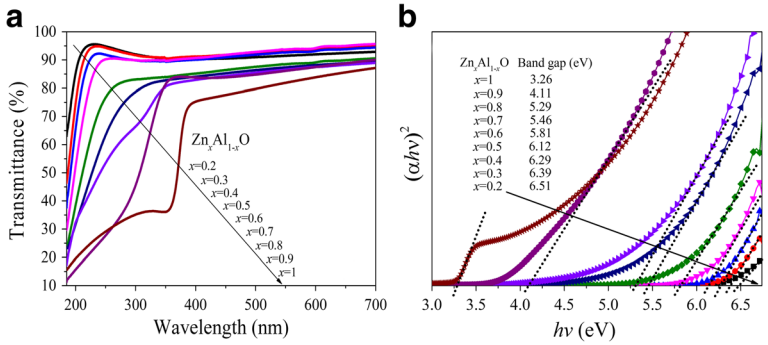

Fig. 2 Transmittance spectra (**a**) and the plots of $(\alpha h\nu)^2$ vs. photon energy (**b**) of $Zn_xAl_{1-x}O$ samples

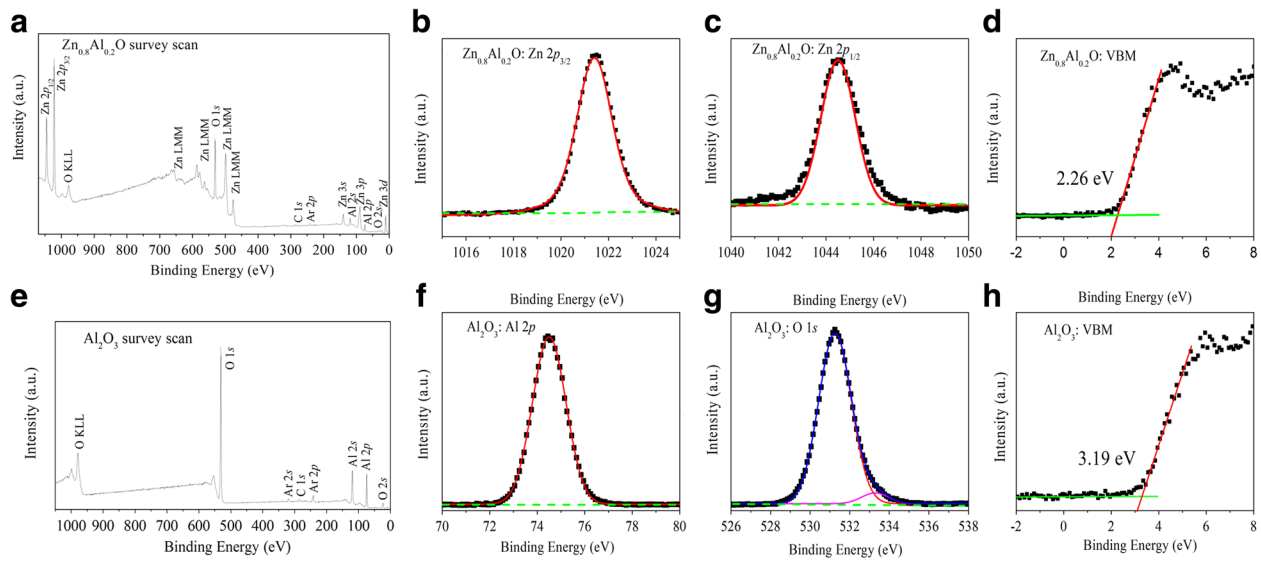

Fig. 3 XPS spectra for **a** survey scan, **b** Zn $2p_{3/2}$, **c** Zn $2p_{1/2}$, and **d** VBM of $Zn_{0.8}Al_{0.2}O$ and **e** survey scan, **f** Al 2*p*, **g** O 1*s*, and **h** VBM of Al_2O_3, with application of a low-energy electron flood gun

leading edge of the valence band spectrum and the background [39], as shown in Fig. 3d,h. This linear method has already been widely used to determine the VBM of semiconductors with high accuracy. The VBM values of atomic-layer-deposited thick $Zn_{0.8}Al_{0.2}O$ and Al_2O_3 samples are 2.26 and 3.19 eV, respectively. The scatter of the data relative to the fit are estimated as an uncertainty in VBM positions of less than 0.03 eV. The parameters deduced from Fig. 3 are summarized in Table 2 for clarity.

Four CLs of $Al_2O_3/Zn_{0.8}Al_{0.2}O$ heterojunction with different Al_2O_3 thickness are shown in Fig. 4. The Al 2*p*, Zn $2p_{1/2}$, and Zn $2p_{3/2}$ XPS spectra in Fig. 4(a, e, i), (b, f, j), and (c, g, k), respectively, are fitted by a single contribution, attributed to the bonding configurations Al-O and Zn-O. For the O 1*s* XPS spectrum in Fig. 4d, h, l, an additional low-intensity higher binding energy component is observed. The extra component is attributed to metal (Al, Zn)-O bonding at the interface and/or inelastic losses to free carries in the Al_2O_3 layer, similar results obtained by previous study [19]. With the increase of the Al_2O_3 thickness, the intensity of Zn $2p_{1/2}$ peak is weakened while the energy resolution is deteriorated shown in Fig. 4f. It is difficult to observe and fit for Al_2O_3 thickness of 5 nm as shown in Fig. 4j. So, the peak position of Zn $2p_{1/2}$ in 5-nm Al_2O_3 sample listed by a bold number in Table 2 is a large deviation as a result of the big error of fitting. The CLs of $Al_2O_3/Zn_{0.8}Al_{0.2}O$ samples are summarized in Table 2.

The ΔE_V of the $Al_2O_3/Zn_{0.8}Al_{0.2}O$ heterojunction is determined from the energy separation between the CLs in the $Al_2O_3/Zn_{0.8}Al_{0.2}O$ sample and the VBM to CLs separations in the thick Al_2O_3 and $Zn_{0.8}Al_{0.2}O$ samples, respectively. Table 3 lists the ΔE_V values for all Al_2O_3 samples with thickness of 3–5 nm, and the error in each value is ± 0.07 eV. Therefore, the averaged ΔE_V value is 0.87 ± 0.22 eV. It is important to note that the calculation does not include the italic numbers in Table 3 because of the big error fitting of CLs of Zn $2p_{1/2}$ in the 5-nm $Al_2O_3/Zn_{0.8}Al_{0.2}O$ sample.

However, there are obvious considerable CL shifts up to 0.6 eV sensitive to the thicknesses of the Al_2O_3 and $Zn_{0.8}Al_{0.2}O$ layers from the given experimental data in Table 2, and different ΔE_V values are obtained in the

Table 2 Peak positions of CLs and VBM positions used to calculate the ΔE_V of the $Al_2O_3/Zn_{0.8}Al_{0.2}O$ heterojunction

	$Zn_{0.8}Al_{0.2}O$	Al_2O_3	3 nm $Al_2O_3/Zn_{0.8}Al_{0.2}O$	4 nm $Al_2O_3/Zn_{0.8}Al_{0.2}O$	5 nm $Al_2O_3/Zn_{0.8}Al_{0.2}O$
Al 2*p*		74.35	74.6	74.93	74.87
O 1*s*		531.1	531.32	531.66	531.63
Zn $2p_{3/2}$	1021.41		1021.69	1022.05	1021.97
Zn $2p_{1/2}$	1044.51		1044.85	*1045.11*	**1045.64**
VBM	2.26	3.19			

The peak position of Zn $2p_{1/2}$ in 5-nm Al_2O_3 sample listed by a bold number

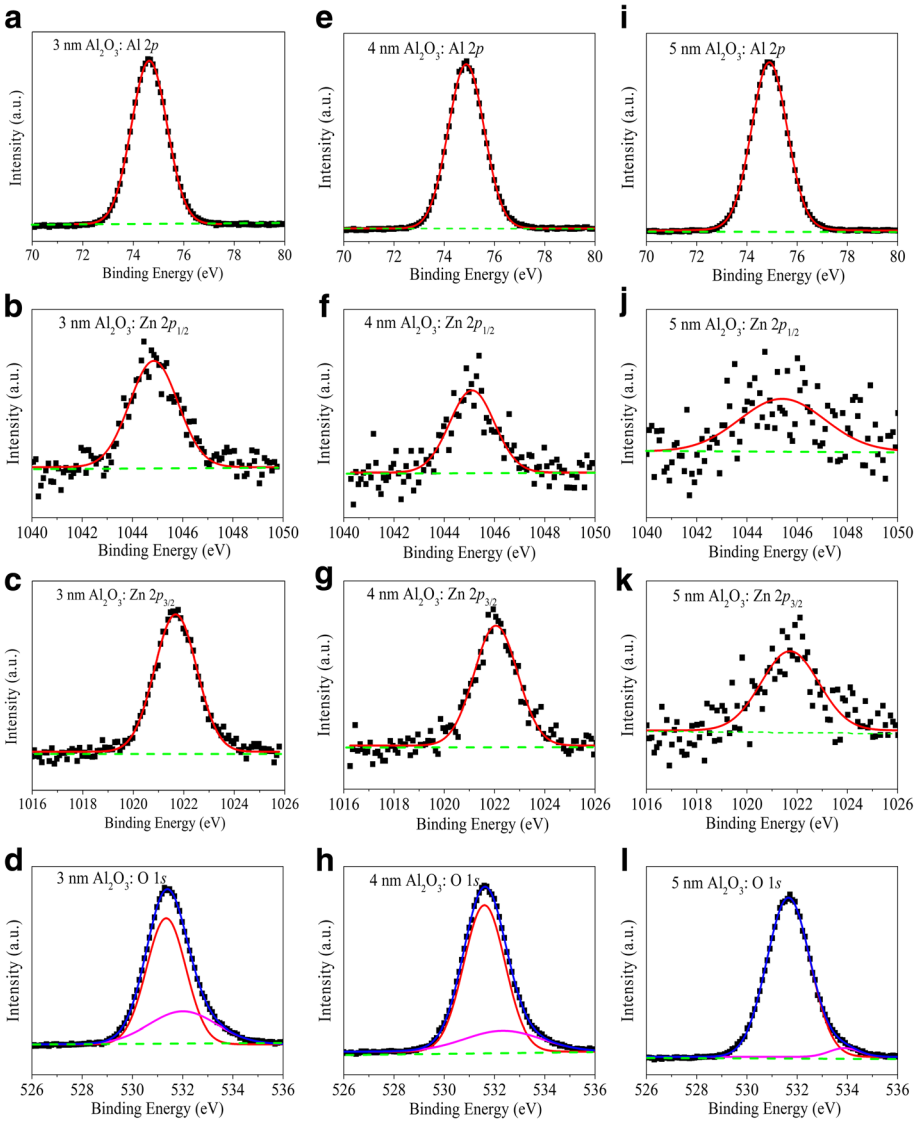

Fig. 4 CLs of $Al_2O_3/Zn_{0.8}Al_{0.2}O$ samples with varied Al_2O_3 thickness **a**–**d** 3 nm, **e**–**h** 4 nm, and **i**–**l** 5 nm, with application of a low-energy electron flood gun

various combinations of XPS CLs in Table 3. It is directly proved that the charging phenomenon generated by the X-ray irradiation results in adverse effects on the ΔE_V determination when taking XPS measurement on insulator/semiconductor heterojunction in spite of operating neutralizing electron gun. As has been widely reported, the influences of differential charging on the band offsets determination cannot be neglected even in very thin oxides. Therefore, zero charging method is adopted in this study in order to eliminate charging-induced errors and recover the accurate ΔE_V value.

The error in the ΔE_V measurement is resulting from the differential charging effect that prevents the correct determination of the energy differences, such as between

Table 3 The ΔE_V values of the $Al_2O_3/Zn_{0.8}Al_{0.2}O$ heterojunction with Al_2O_3 thickness of 3–5 nm

ΔE_V	3 nm $Al_2O_3/Zn_{0.8}Al_{0.2}O$		4 nm $Al_2O_3/Zn_{0.8}Al_{0.2}O$		5 nm $Al_2O_3/Zn_{0.8}Al_{0.2}O$	
	Zn $2p_{3/2}$	Zn $2p_{1/2}$	Zn $2p_{3/2}$	Zn $2p_{1/2}$	Zn $2p_{3/2}$	Zn $2p_{1/2}$
Al $2p$	0.9	0.84	0.87	0.91	0.89	*0.32*
O 1 s	0.87	0.81	0.85	0.89	0.9	*0.33*

The calculation does not include the italic numbers

the Al 2*p* and Zn $2p_{3/2}$ signals even in very thin Al_2O_3 films in heterojunction. In Fig. 5, the binding energies of the Al 2*p*, Zn $2p_{3/2}$, and Zn $2p_{1/2}$ CLs for the 3, 4, 5, and 8 nm Al_2O_3 films are plotted as a function of X-ray irradiation time. The binding energies of Al 2*p*, Zn $2p_{3/2}$, and Zn $2p_{1/2}$ CLs of the 3-nm Al_2O_3 sample in Fig. 5a increase slowly until they stabilize on a steady state value of 74.63 ± 0.01, 1021.77 ± 0.01, and 1044.83 ± 0.02 eV, respectively. Similar time dependencies are observed in the 4-, 5-, and 8-nm Al_2O_3 films, as shown in Fig. 5b–d. The results show that CL steady state spectra are obtained after stabilization of the signals in the heterojunction-considered charge saturated when X-ray irradiation time is more than 25 min. Therefore, X-ray irradiation time is one of the most important parameters to determine the insulator/semiconductor band offsets. Layer thickness dependence in peak positions is mainly resulting from the differential charging effects. True peak positions can be acquired by extrapolating the measured binding energies to zero oxide thickness and ideally to zero charge, similar results are reported for SiO_2/Si [25], HfO_2/Si [26], and MgO/$Zn_{0.8}Al_{0.2}O$ [19] systems.

The CLs positions of the Al 2*p*, Zn $2p_{1/2}$, and Zn $2p_{3/2}$ are plotted as a function of the Al_2O_3 film thickness, as shown in Fig. 6. By linear fitting of the experimental data, the CLs positions of the Al 2*p*, Zn $2p_{1/2}$, and Zn $2p_{3/2}$ peaks are determined to be 74.51 ± 0.03, 1044.77 ± 0.06, and 1021.7 ± 0.04 eV, respectively. In order to correct the ΔE_V of the $Al_2O_3/Zn_{0.8}Al_{0.2}O$ heterojunction, we calculate the energy differences between the extrapolated (Al 2*p*, Zn $2p_{1/2}$) and (Al 2*p*, Zn $2p_{3/2}$) at zero thickness. The values are 970.26 ± 0.07 and 947.19 ± 0.05 eV, respectively. Inserting these values in Eq. (1), the ΔE_V are calculated to be 0.83 ± 0.09 and 0.8 ± 0.08 eV, which is in good agreement using the two combinations of CLs of the $Al_2O_3/Zn_{0.8}Al_{0.2}O$ heterojunction. Therefore, the averaged ΔE_V value is 0.82 ± 0.12 eV.

There are three possible reasons that affect the ΔE_V values in addition to the XPS method itself. Firstly, the oxide stoichiometry of the Al_2O_3 thin films measured by XPS is almost the same in the different Al_2O_3 samples with thickness of 3–8 nm. Therefore, the composition of the Al_2O_3 film is independent of thickness and the binding energy shifts in Fig. 5 is related to the differential charging effect occurring in the $Al_2O_3/Zn_{0.8}Al_{0.2}O$ heterojunction during X-ray irradiation. Secondly, band bending at the heterointerface could induce a systematic error in determination of ΔE_V, and we check that this error is much smaller than the average standard deviation of ± 0.03 eV given above. Finally, the strain existing in the Al_2O_3 overlayer of the heterojunction will induce

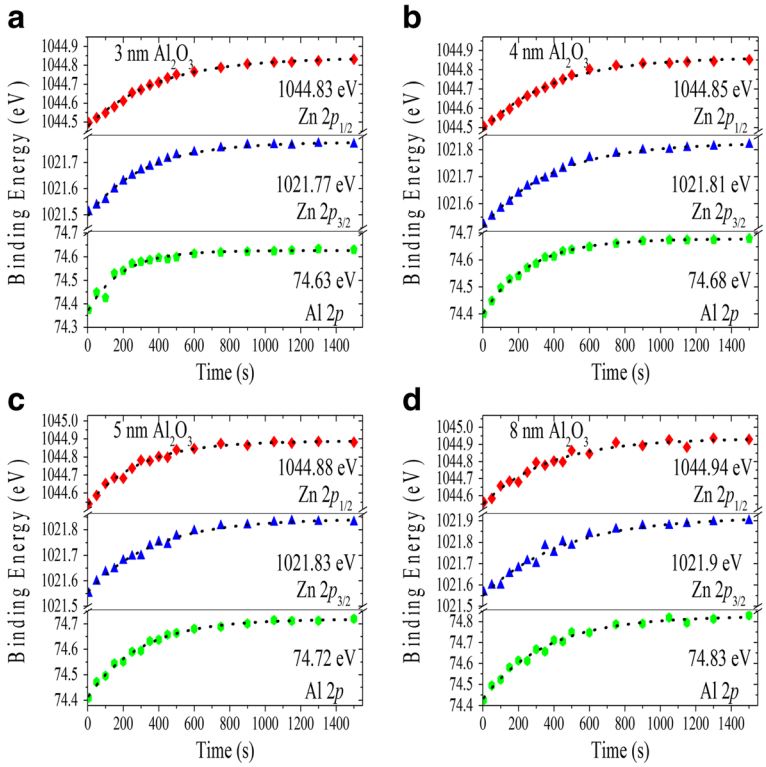

Fig. 5 Time-resolved plots showing the respective binding energies vs. X-ray irradiation time for **a** 3 nm, **b** 4 nm, **c** 5 nm, and **d** 8 nm Al_2O_3 films on $Zn_{0.8}Al_{0.2}O$ on Si substrates, with application of a low-energy electron flood gun

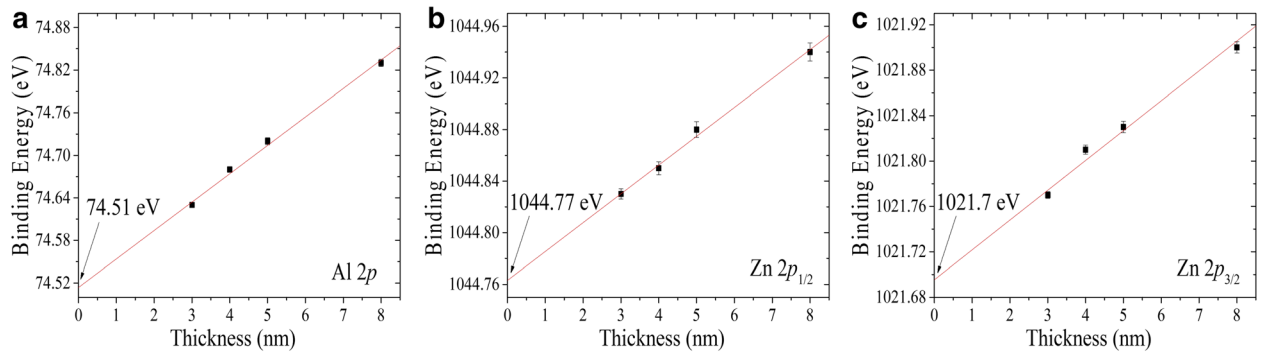

Fig. 6 Al 2*p* (**a**), Zn $2p_{1/2}$ (**b**), and Zn $2p_{3/2}$ (**c**), CL binding energies as a function of the Al_2O_3 thin film thickness

a piezoelectric field that probably affects the measured ΔE_V value, a similar phenomenon explained by Martin et al [40]. The heterojunction underlayer $Zn_{0.8}Al_{0.2}O$ is thick enough, and the structure of both materials is amorphous. Therefore, the strain-induced piezoelectric field is not taken into consideration in this study.

To infer the ΔE_C based on the value of ΔE_V, we need to know the E_g of the ultrathin Al_2O_3 layer, which can be estimated from O 1*s* core-level binding energy spectrum of atomic-layer-deposited Al_2O_3 thin films with energy loss structure. The binding energy is calculated from the difference in the total photoelectron energy minus the kinetic energy due to the loss in photoelectron energy by inelastic collision processes within the sample. The minimum inelastic loss is equal to the band gap energy, and the most cited value of E_g is 6.8 eV [41–43]. Together with the $Zn_{0.8}Al_{0.2}O$ E_g of 5.29 eV at room temperature, the ΔE_C can be simply derived by the equation, $\Delta E_C = E_g(Al_2O_3) - \Delta E_V - E_g(Zn_{0.8}Al_{0.2}O)$, where $E_g(Al_2O_3)$ and $E_g(Zn_{0.8}Al_{0.2}O)$ are the band gaps of the Al_2O_3 and $Zn_{0.8}Al_{0.2}O$ thin films, respectively. The ΔE_C is calculated to be 0.69 ± 0.12 eV, which means that the barrier height for transport of electrons is smaller than that of holes. The band alignment of the $Al_2O_3/Zn_{0.8}Al_{0.2}O$ heterojunction obtained from XPS measurements is shown in Fig. 7. The CBM of Al_2O_3 is higher than that of $Zn_{0.8}Al_{0.2}O$; however, the VBM of Al_2O_3 is lower than that of $Zn_{0.8}Al_{0.2}O$. Therefore, a nested type-I band alignment with a ratio $\Delta E_C/\Delta E_V$ of about 1:1.2 is obtained.

Usually, the MCP gain under direct current (DC) mode is limited by the space charge density without consideration of ion feedback, and the recharge time constant or dead time (τ) is several milliseconds [44]. When operating a MCP as a DC current amplifier, the gain is constant until the output current (I_{oc}) exceeds about 10% of the strip current through the plate. However, the MCP works in a highly saturated state under a photon-counting mode, and the electron avalanche multiplication is done within several nanoseconds that is a million times faster than τ [44–46]. The peak output current in pulsed operation exceeding the I_{oc} by several orders of magnitude is observed. Therefore, anode signal charges probably come from the tunneling electrons in the $Al_2O_3/Zn_xAl_{1-x}O$ heterojunction of the inner wall of the MCP. For photon-counting mode, both ΔE_V and ΔE_C should be sufficiently large, which can prevent the thermal excitation of electrons generated from the SEE layer into the electron multiplier system that probably produces high electronics dark noise and result in a reduced signal to noise ratio. The present result has no effects on the MCP operating under DC mode which is determined by space charge saturation, but has negative effects on the photon-counting mode which needs a type-II heterojunction to improve tunneling probability for excellent performance. The relationship between the $Al_2O_3/Zn_xAl_{1-x}O$ heterojunction and charge replenishment

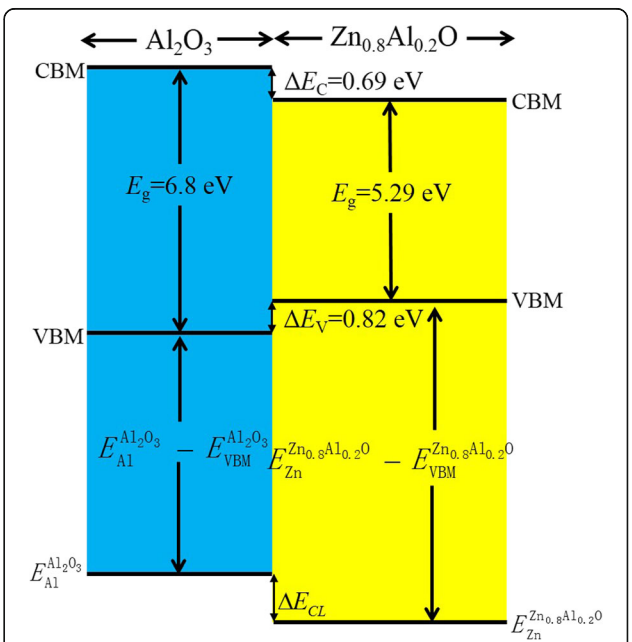

Fig. 7 The schematic diagram of band offset at the $Al_2O_3/Zn_{0.8}Al_{0.2}O$ heterojunction interface

mechanism under photon-counting mode needs further study. Therefore, the band alignment of the Al_2O_3/$Zn_xAl_{1-x}O$ heterojunction should be constructed and adjusted by appropriately changing the ratio of Al and Zn elements under the premise of meeting the requirements of the electron multiplier.

Conclusions

The structure and optical band gaps of $Zn_xAl_{1-x}O$ ($0.2 \le x \le 1$) films deposited by atomic layer deposition are investigated. And the band offset measurements of the $Al_2O_3/Zn_{0.8}Al_{0.2}O$ heterojunction have been determined by XPS with zero charging method. The results show that X-ray irradiation time is one of the most important parameters to determine the band offsets. The layer thickness dependence in peak positions is mainly derived from the differential charging effects, and true peak positions are obtained by extrapolating the measured binding energies to zero oxide thickness and ideally to zero charge. The ΔE_V value is obtained to be 0.82 ± 0.12 eV, and the corresponding ΔE_C is calculated to be 0.69 ± 0.12 eV. Therefore, a nested type-I band alignment is obtained. Understanding of the band alignment parameters of the $Al_2O_3/Zn_{0.8}Al_{0.2}O$ interface will facilitate the knowledge of their carrier transport mechanism and design of corresponding hybrid devices, especially in the research process of electron multipliers.

Abbreviations

Al_2O_3: Aluminum oxide; ALD: Atomic layer deposition; CBM: Conduction band minimum; CLs: Core levels; DC: Direct current; DEZ: Diethylzinc; E_g: Band gap; I_{oc}: Output current; MCP: Microchannel plate; MgO: Magnesium oxide; SEE: Secondary electron emission; TMA: Trimethylaluminum; VBM: Valence band maximum; XPS: X-ray photoelectron spectroscopy; XRD: X-ray diffractometer; $Zn_xAl_{1-x}O$: Zinc aluminum oxide; ΔE_C: Conduction band offset; ΔE_V: Valence band offset

Acknowledgements

We express our sincere gratitude to the reviewer, who has given us the most valuable advice. We thank Dr. Lin Wang and Dr. Hailiang Nie for the meaningful discussions on XRD measurement and chemical formula of $Zn_{0.8}Al_{0.2}O$, respectively. We are especially grateful to Danjiao Wang for her careful reading and polishing the manuscript.

Funding

This work was supported by the National Natural Science Foundation of China (Nos. 11675278 and 11535014), the Strategic Priority Research Program of the Chinese Academy of Sciences (No. XDA10010400), and the Beijing Municipal Science and Technology Project (No. Z171100002817004).

Availability of Data and Materials

The raw data used in this study is not available for the time being, because the data has not been fully analyzed, and the results of the analysis will be gradually introduced in the recent published articles.

Authors' Contributions

BY designed and conducted the experiments and drafted the manuscript. YY, YY and KW prepared the thin films and performed the XRD, UV-Vis-IR and XPS measurements. SL and YH provided the technical support and advices on the work. All authors read and approved the final manuscript.

Competing Interests

The authors declare that they have no competing interests.

Publisher's Note

Author details

[1]State Key Laboratory of Particle Detection and Electronics, Institute of High Energy Physics of Chinese Academy of Sciences, Beijing 100049, People's Republic of China. [2]Department of Physics, Nanjing University, Nanjing 210093, People's Republic of China. [3]School of Science, Xi'an University of Technology, Xi'an 710048, People's Republic of China. [4]University of Chinese Academy of Sciences, Beijing 100049, People's Republic of China.

Received: 24 December 2016 Accepted: 8 May 2017
Published online: 19 May 2017

References

1. Mane AU, Peng Q, Elam JW et al (2012) An atomic layer deposition method to fabricate economical and robust large area microchannel plates for photodetectors. Physics Procedia 37:722–732
2. Yan BJ, Liu SL, Heng YK (2015) Nano-oxide thin films deposited via atomic layer deposition on microchannel plates. Nanoscale Res Lett 10:11
3. Jana D, Maikap S, Tien TC et al (2012) Formation-polarity-dependent improved resistive switching memory performance using $IrO_x/GdO_x/WO_x/W$ structure. Jpn J Appl Phys 51:6
4. Petric P, Bevis C et al (2010) Reflective electron beam lithography: a maskless ebeam direct write lithography approach using the reflective electron beam lithography concept. J Vac Sci Technol B 28:C6C6
5. Siegmund OHW, McPhate JB, Tremsin AS et al (2012) Atomic layer deposited borosilicate glass microchannel plates for large area event counting detectors. Nucl Instrum Methods Phys Res Sect A 695:168–171
6. Yang YZ, Liu SL, Zhao TC, YAN BJ et al (2016) Single electron counting using a dual MCP assembly. Nucl Instrum Methods Phys Res Sect A 830:438–443
7. George SM (2010) Atomic layer deposition: an overview. Chem Rev 110:111–131
8. Makino T, Segawa Y, Kawasaki M (2001) Band gap engineering based on $Mg_xZn_{1-x}O$ and $Cd_yZn_{1-y}O$ ternary alloy films. Appl Phys Lett 78:1237–1239
9. Hummer K (1973) Interband magnetoreflection of ZnO. Phys Status Solidi B-Basic Res 56:249–260
10. Ke Y, Lany S, Berry JJ et al (2014) Enhanced electron mobility due to dopant-defect pairing in conductive ZnMgO. Adv Funct Mater 24:2875–2882
11. Kumar P, Malik HK, Ghosh A et al (2013) Bandgap tuning in highly c-axis oriented $Zn_{1-x}Mg_xO$ thin films. Appl Phys Lett 102:5
12. Yao G, Tang YQ, Fu YJ et al (2015) Fabrication of high-quality ZnCdO epilayers and ZnO/ZnCdO heterojunction on sapphire substrates by pulsed laser deposition. Appl Surf Sci 326:271–275
13. Lee CS, Cuong HB et al (2015) Comparative study of group-II alloying effects on physical property of ZnGaO transparent conductive films prepared by RF magnetron sputtering. J Alloy Compd 645:322–327
14. Mane AU, Elam JW (2013) Atomic layer deposition of $W:Al_2O_3$ nanocomposite films with tunable resistivity. Chem Vapor Depos 19:186–193
15. Tong WM, Brodie AD, Mane AU et al (2013) Nanoclusters of MoO_{3-x} embedded in an Al_2O_3 matrix engineered for customizable mesoscale resistivity and high dielectric strength. Appl Phys Lett 102:5
16. Elam JW, Routkevitch D, George SM (2003) Properties of ZnO/Al_2O_3 alloy films grown using atomic layer deposition techniques. J Electrochem Soc 150:G339–G347
17. Lapington JS, Thompson DP, May PW et al (2009) Investigation of the secondary emission characteristics of CVD diamond films for electron amplification. Nucl Instrum Methods Phys Res Sect A 610:253–257
18. Jokela SJ, Veryovkin IV, Zinovev AV et al (2012) Secondary electron yield of emissive materials for large-area micro-channel plate detectors: surface composition and film thickness dependencies. In: Liu T (ed) Proceedings of the 2nd International Conference on Technology and Instrumentation in Particle Physics. Elsevier Science Bv, Amsterdam, pp 740–747
19. Yan BJ, Liu SL, Yang YZ, Heng YK (2016) Band alignment of atomic layer deposited $MgO/Zn_{0.8}Al_{0.2}O$ heterointerface determined by charge corrected X-ray photoelectron spectroscopy. Appl Surf Sci 371:118–128

20. Kraut EA, Grant RW et al (1983) Semiconductor core-level to valence-band maximum binding-energy differences: precise determination by X-ray photoelectron-spectroscopy. Phys Rev B 28:1965–1977
21. Alay JL, Hirose M (1997) The valence band alignment at ultrathin SiO_2/Si interfaces. J Appl Phys 81:1606
22. Grunthaner FJ, Grunthaner PJ (1986) Chemical and electronic structure of the SiO_2/Si interface. Materials Science Reports 1:65–160
23. Seguini G, Perego M, Spiga S et al (2007) Conduction band offset of HfO_2 on GaAs. Appl Phys Lett 91:3
24. Tanimura T, Toyoda S, Kamada H et al (2010) Photoinduced charge-trapping phenomena in metal/high-k gate stack structures studied by synchrotron radiation photoemission spectroscopy. Appl Phys Lett 96:3
25. Iwata S, Ishizaka A (1996) Electron spectroscopic analysis of the SiO_2/Si system and correlation with metal-oxide-semiconductor device characteristics. J Appl Phys 79:6653–6713
26. Perego M, Seguini S (2011) Charging phenomena in dielectric/semiconductor heterostructures during X-ray photoelectron spectroscopy measurements. J Appl Phys 110:11
27. Hilmi I, Thelander E, Schumacher P et al (2016) Epitaxial $Ge_2Sb_2Te_5$ films on Si(111) prepared by pulsed laser deposition. Thin Solid Films 619:81–85
28. Pandikunta M, Ledyaev O, Kuryatkov V et al (2014) Structural analysis of N-polar AlN layers grown on Si (111) substrates by high resolution X-ray diffraction. Phys Status Solidi C 11:487–490
29. Tynell T, Yamauchi H, Karppinen M et al (2013) Atomic layer deposition of Al-doped ZnO thin films. J Vac Sci Technol A 31:4
30. Tauc J (1966) The Optical Properties of Solids. Academic, Waltham
31. Dar TA, Agrawal A, Misra P et al (2014) Valence and conduction band offset measurements in $Ni_{0.07}Zn_{0.93}O$/ZnO heterostructure. Curr Appl Phys 14:171–175
32. Dhakal T, Vanhart D, Christian R et al (2012) Growth morphology and electrical/optical properties of Al-doped ZnO thin films grown by atomic layer deposition. J Vac Sci Technol A 30:10
33. Dhakal TP, Peng CY, Tobias RR et al (2014) Characterization of a CZTS thin film solar cell grown by sputtering method. Sol Energy 100:23–30
34. Zhu BL, Lu K, Wang J et al (2013) Characteristics of Al-doped ZnO thin films prepared in Ar + H_2 atmosphere and their vacuum annealing behavior. J Vac Sci Technol A 31:9
35. Moulder JF, Stickle WF (1992) Sobol PE et al Handbook of X-ray photoelectron spectroscopy. PerkinElmer Corp, Eden Priarie
36. Scofield JH (1976) Hartree-slater subshell photoionization cross-sections at 1254 and 1487 eV. J Electron Spectrosc Relat Phenom 8:129–137
37. Tanuma S, Powell CJ, Penn DR (1994) Calculations of electron inelastic mean free paths. 5. Data for 14 organic compounds over the 50–2000 eV range. Surf Interface Anal 21:165–176
38. Wu Y, Hermkens PM, van de Loo BWH et al (2013) Electrical transport and Al doping efficiency in nanoscale ZnO films prepared by atomic layer deposition. J Appl Phys 114:024308
39. Chambers SA, Droubay T, Kaspar TC et al (2004) Experimental determination of valence band maxima for $SrTiO_3$, TiO_2, and SrO and the associated valence band offsets with Si(001). J Vac Sci Technol B 22:2205–2215
40. Martin G, Botchkarev A, Rockett A et al (1996) Valence-band discontinuities of wurtzite GaN. AlN, and InN heterojunctions measured by X-ray photoemission spectroscopy, Appl Phys Lett 68:2541–2543
41. Kamimura T, Sasaki K, Hoi Wong M et al (2014) Band alignment and electrical properties of Al_2O_3/β-Ga_2O_3 heterojunctions. Appl Phys Lett 104:192104
42. Huang ML, Chang YC, Chang YH et al (2009) Energy-band parameters of atomic layer deposited Al_2O_3 and HfO_2 on $In_xGa_{1-x}As$. Appl Phys Lett 94:3
43. Liu JS, Clavel M, Hudait MK (2015) Tailoring the valence band offset of Al_2O_3 on epitaxial $GaAs_{1-y}Sb_y$ with tunable antimony composition. ACS Appl Mater Interfaces 7:28624–28631
44. Wiza JL (1979) Microchannel plate detectors. Nuclear Instruments and Methods 162:587–601
45. Adams B, Chollet M, Elagin A et al (2013) A test-facility for large-area microchannel plate detector assemblies using a pulsed sub-picosecond laser. Rev Sci Instrum 84:061301
46. Siegmund OHW, McPhate JB, Jelinsky SR et al (2013) Large area microchannel plate imaging event counting detectors with sub-nanosecond timing. IEEE Trans Nucl Sci 60:923–931